machines

MDPI

Article

Innovative Design and Performance Study of a Carbon-Fiber-Wound Reinforced Metal Seal Tube for Ultra-High-Pressure Hydrogen Solenoid Valve

Shanhai Mao [1,*], Guoyun Gu [1], Changbo Shi [2], Tiexiang Wang [2], Tianci Fan [3], Tiantian Huang [3] and Kaichen Song [3]

[1] Yuyao Sanlixin Solenoid Valve Co., Ltd., Yuyao 315400, China; sanlixin@solenoidvalve.cn
[2] Huanjiang Laboratory, Zhuji 311800, China; hjscb@huanjianglab.cn (C.S.); hjwtx@huanjianglab.cn (T.W.)
[3] School of Aeronautics and Astronautics, Zhejiang University, Hangzhou 310027, China; tcfan@zju.edu.cn (T.F.); tthuang@zju.edu.cn (T.H.); kcsong@zju.edu.cn (K.S.)
* Correspondence: maoshanhai@solenoidvalve.cn

Abstract

A 70 MPa class hydrogen solenoid valve needs a metal seal tube with a high strength margin at the specified safety factor (proof pressure 175 MPa). A lightweight scheme is therefore proposed in which the thin-walled tube is reinforced by carbon-fiber hoop winding. S31603 austenitic stainless steel is ordinarily selected as the primary material for this pressure-bearing component owing to its excellent corrosion resistance and favorable hydrogen-embrittlement resistance. However, its low yield strength means that satisfying the strength requirement only by increasing the wall thickness would raise the structural mass, widen the non-magnetic gap and reduce the electromagnetic efficiency. To avoid this, a thin-walled S31603 tube is used as the metallic liner, and a mechanical model of the metal–composite structure is established on the basis of composite netting theory and thick-walled cylinder elasticity. The winding-layer thickness and the process parameters are then determined, and the design is verified by finite element analysis and pressure testing. The results show that, at the 175 MPa proof pressure, a 3 mm thick all-metal seal tube has an elastic limit of only about 65.4 MPa, far below the requirement. After carbon-fiber wet winding, the composite seal tube reaches the required strength, with a total wall thickness of only about 3 mm and a much lower mass. Because the carbon-fiber layer is non-magnetic, the structure improves the pressure-bearing capacity while introducing almost no additional reluctance. It effectively decouples the contradiction between the structural strength and the magnetic-circuit efficiency and offers a new route for the lightweight design of hydrogen fluid-control components.

Keywords: ultra-high-pressure solenoid valve; carbon-fiber winding; composite material; composite netting theory; wet filament winding; mechanical design; finite element analysis

Check for updates

Academic Editors: Jose E. Ruiz-Sarrio, Claudia Martis and Jose Alfonso Antonino-Daviu

Received: 17 September 2026
Revised: 14 October 2026
Accepted: 14 October 2026
Published: 22 October 2026

Copyright: © 2026 by the authors. Licensee MDPI, Basel, Switzerland. This article is an open access article distributed under the terms and conditions of the Creative Commons Attribution (CC BY) license.

1. Introduction

Driven by the carbon-peak and carbon-neutrality strategic goals, the hydrogen-energy industry, and hydrogen fuel-cell vehicles in particular, is developing rapidly. Because of its relatively high storage density and its relatively simple infrastructure requirements, high-pressure gaseous hydrogen storage has become the mainstream hydrogen storage route for fuel-cell vehicles [1]. An onboard hydrogen storage system consists of a high-pressure hydrogen storage vessel and fluid-control components such as cylinder valves and pipeline

valves. Such a system operates at high pressure with a flammable and explosive medium, and its pressure-bearing components are at risk of hydrogen-embrittlement failure, which places stringent demands on the safety design [2,3]. As a core element that controls the on/off of hydrogen flow in the pipeline, the solenoid valve directly governs the safety, efficiency and response speed of the whole vehicle system.

The key component that withstands the internal pressure in an ultra-high-pressure solenoid valve is the metal seal tube, which is usually made of 316L [4,5]. 316L is the commercial designation of the same material as S31603, i.e., UNS S31603, which is specified in ASTM A479/A479M-25 [6]. This steel shows good corrosion resistance, good machinability and low susceptibility to hydrogen embrittlement in a high-pressure hydrogen environment, and it is therefore a primary candidate material for hydrogen-system pressure-bearing components [7]. At an operating pressure of 70 MPa and a safety factor of 2.5, the proof pressure is 175 MPa [8]. Under this condition, the relatively low yield strength of S31603 (170 MPa) makes it difficult to satisfy the strength requirement of a thin-walled structure. Thick-walled cylinder theory gives an elastic pressure-bearing limit of only about 65.4 MPa for a 3 mm thick all-metal seal tube. This value is below the 70 MPa operating pressure and far below the 175 MPa proof pressure, so the strength requirement cannot be met. Simply increasing the wall thickness raises the structural mass. When the seal tube is part of the magnetic circuit, a thicker wall also widens the non-magnetic gap and increases the reluctance. A larger magnetomotive force is then required to produce the same electromagnetic force. This increases the energy consumption and the temperature rise. It also slows the dynamic response. A contradiction therefore arises between the structural strength and the magnetic-circuit efficiency.

To resolve this contradiction, researchers have investigated the problem from several angles. Wang Jianzhong et al. [9] established an FEA model for the electromagnetic force of a solenoid valve based on ANSYS Multiphysics (ANSYS 2022 R2). The model calculates the magnetic field distribution in the magnetic circuit, the flux-leakage effect, and the electromagnetic force on the armature. It provides an effective tool for magnetic-circuit parameter design. Wang Hong et al. [10] considered the fringe flux at the air gap, material magnetic saturation, and flux leakage. They established a mathematical model of the electromagnetic attraction force of a solenoid valve for hydrogen vehicles. On this basis, the structural parameters were optimized. The results indicate that a smaller air gap and an improved magnetic-circuit structure increase the electromagnetic attraction force and improve the dynamic response. These studies indicate that the non-magnetic gap should be minimized while the pressure-bearing strength is ensured. This is the key to improving solenoid-valve performance.

Material substitution is another route. High-nitrogen austenitic stainless steel has low permeability. Its yield strength is about 2 to 4 times that of standard 316-type steel. However, its melting and plastic forming are difficult [11]. Nickel-based alloys such as Inconel 625 have also been studied for hydrogen-tank solenoid-valve components such as the valve stem [12]. However, their high cost limits wide engineering adoption.

The carbon-fiber-wound metallic liner composite structure is an alternative reinforcement route. It has been widely applied to high-pressure hydrogen storage vessels. Zheng Chuanxiang et al. [13] established a mechanical analysis model of a carbon-fiber-wound aluminum-liner hydrogen vessel. The model is based on composite netting theory and classical composite plate theory. They also proposed a fiber-preload control method to optimize the stress distribution. Zhan Helin et al. [14] carried out finite element stress analysis and hydrostatic burst tests on a 70 MPa aluminum-liner fully wound carbon-fiber cylinder for vehicles. Their results show that the winding layer bears most of the hoop load. The aluminum-liner stress remains within a safe range. The minimum burst pressure

reached 2.35 times the nominal working pressure. A recent study evaluated the hydrogen compatibility and the fatigue life of a steel-liner/CFRP hoop-wound (Type 2) vessel [15]. The study covered working pressures up to 93 MPa in a high-pressure hydrogen environment. These studies confirm that the winding layer can carry the dominant hoop stress. This can substantially reduce the structural mass. However, the applicability of this composite structure to the solenoid-valve seal tube remains to be examined. Its compatibility with the magnetic-circuit performance has not yet been systematically reported.

Carbon-fiber-reinforced polymers offer a high specific strength and specific stiffness and are non-magnetic, which is why they are widely used in aerospace, high-pressure cylinders and other fields [1,13]. Inspired by these characteristics, this paper proposes a lightweight structure in which a thin-walled metal seal tube is reinforced by hoop-wound carbon fiber, so that the thin-walled metal tube retains the sealing, connection and magnetic-circuit conduction functions while the external winding layer carries the dominant hoop load. The study addresses the following: a mechanical model of the metal-composite structure is established from composite netting theory and thick-walled cylinder elasticity, from which the thickness of the composite layer is determined; the static strength of the designed structure is checked using the finite element method; and the process parameters of the composite tube are determined, its load-bearing performance is verified by pressure testing, and the effect on the magnetic-circuit performance is analyzed. The aim is to provide a reference for the lightweight design of pressure-bearing components of hydrogen solenoid valves at pressure levels of 70 MPa and above.

2. Structure and Design Parameters of the Composite Seal Tube

2.1. Overall Design (Structure and Working Principle of the Ultra-High-Pressure Solenoid Valve)

The high-pressure switching solenoid valve is a key actuator of the hydrogen control system, realizing the on/off control of hydrogen through electromagnetic force. When the coil is energized, the electromagnetic field drives the moving iron core upward, lifting the lower end of the valve needle and thus opening the flow channel. When the coil is de-energized, the magnetic field disappears, and the moving iron core and valve needle return to their initial position under the action of the return spring, thereby closing the flow channel. The structure of the solenoid valve is shown in Figure 1a.

Under ultra-high-pressure conditions above 70 MPa, the seal tube is the key component directly withstanding internal pressure, and its material selection must simultaneously satisfy the strength and non-magnetic requirements. The seal tube is usually made of a high-strength non-magnetic metal. However, when the system medium is high-pressure hydrogen, the material must also have good hydrogen-embrittlement resistance, and austenitic stainless steel is generally recommended in engineering practice. Nevertheless, because the strength of austenitic stainless steel is relatively low, ensuring structural safety under the constraints of mass and volume becomes a design challenge.

To this end, this study abandons the conventional approach of increasing the wall thickness to obtain strength and instead proposes the design concept of functional separation and synergistic reinforcement. As shown in Figure 1b, the composite seal tube consists, from the inside to the outside, of a metallic liner layer and a composite reinforcement layer.

The metallic liner layer is made of S31603 stainless steel by precision machining and is a thin-walled cylinder. It mainly fulfills three functions. First, it provides gas tightness to ensure no leakage of the high-pressure medium. Second, it serves as the winding mandrel, providing a smooth and stable geometric substrate for the external fiber winding [16]. Third, it can be integrated into the magnetic circuit when required. By virtue of its thin wall and small reluctance, it couples efficiently with the external magnetically permeable shell to form a low-reluctance magnetic circuit.

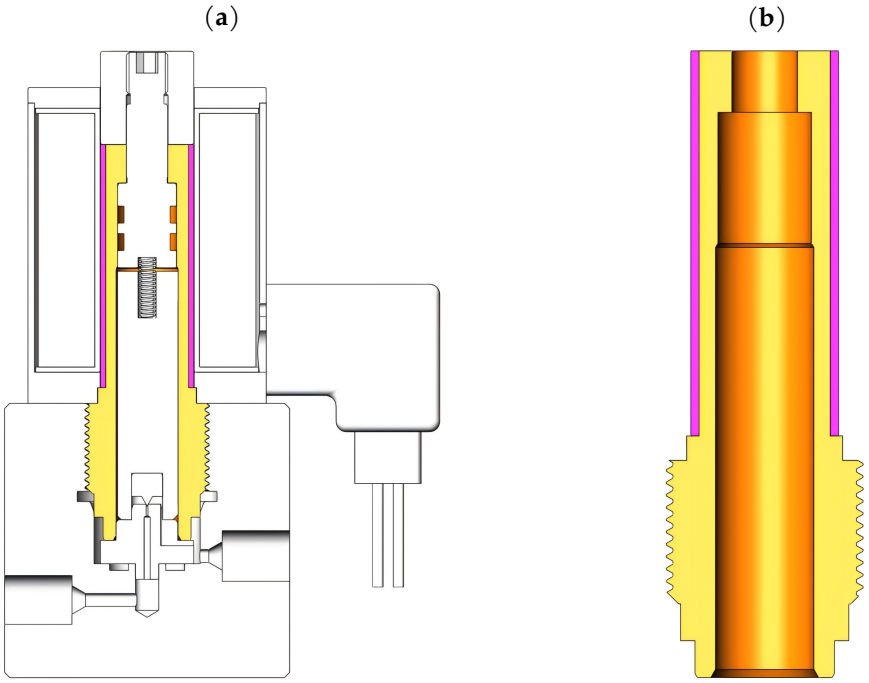


Figure 1. Structural schematics of the high-pressure switching solenoid valve (**a**) and the composite seal tube (**b**). The composite seal tube is one of the components enclosed in the valve shown in (**a**).

The composite reinforcement layer is formed by densely hoop winding an epoxy-resin-impregnated high-strength carbon fiber onto the outer surface of the metallic liner through a wet filament-winding process [17]. It mainly carries the hoop load. On the one hand, it uses the extremely high axial tensile strength of the carbon fiber to resist the dominant stress induced by the internal pressure [18]. On the other hand, it provides the metallic liner with overall stiffness and stability, constraining its radial deformation.

The core advantage of this configuration is that, by exploiting the extremely high specific strength and specific stiffness of the composite, a substantial improvement in load-bearing capacity is achieved at a minimal cost in thickness and mass [19]. Furthermore, because the reinforcement layer is a non-magnetic material, it does not disturb the internal magnetic field distribution of the solenoid valve, thereby decoupling the design constraints between mechanical strength and electromagnetic performance.

2.2. Material and Geometric Parameters

The composite seal tube consists of a thin-walled S31603 stainless steel liner and a carbon-fiber composite reinforcement layer. Its material and geometric parameters are listed in Table 1.

Table 1. Material and geometric parameters of the composite seal tube.

Metallic Liner	**Composite Reinforcement Layer**	**Design Load**
Material: S31603 stainless steel (ASTM A479/A479M-25 [6])	Fiber: Toho Tenax HTA40 E15 1K carbon fiber (1000 filaments per tow) [20]	Working pressure: 70 MPa
Yield strength: 170 MPa	Filament diameter: 7 μm	Gas-tightness test pressure: 105 MPa ($1.5\,p_{op}$ [21])
Elastic modulus: 195 GPa	Tensile strength: 4100 MPa	Proof pressure: 175 MPa ($2.5\,p_{op}$ [21])

Table 1. *Cont.*

Metallic Liner	Composite Reinforcement Layer	Design Load
Poisson's ratio: 0.30	Tensile modulus: 240 GPa	
Inner radius: 6 mm	Matrix: two-component epoxy resin	
Outer radius: 8 mm	Winding process: wet hoop winding	
Wall thickness: 2 mm		Winding-section length L

The yield strength of the metallic liner is taken from the material certificate. The fiber tensile strength and tensile modulus are typical values of the Toho Tenax HTA40 E15 1K carbon fiber (Teijin Carbon, Tokyo, Japan) and are subject to the supplier's certificate. The winding-section length, resin grade, and curing schedule are determined according to the actual design of the seal tube. The gas-tightness test pressure is 105 MPa (1.5 times the working pressure), while the proof pressure is 175 MPa (2.5 times the working pressure). GB/T 42536-2023 [21], Assembly Valve on High Pressure Hydrogen Storage Cylinder for Vehicles, requires a gas-tightness test pressure of at least 1.25 times the working pressure (87.5 MPa). A stricter value of 1.5 times the working pressure is adopted here. The same standard requires a proof pressure of at least 2.5 times the working pressure for high-pressure hydrogen valves. This pressure is used for structural design, finite element verification, and hydrostatic proof testing. The seal tube must not collapse plastically as a whole under it.

3. Mechanical Calculation and Analysis

3.1. Strength Calculation of the All-Metal Seal Tube

The designed wall thickness of the all-metal seal tube is 3 mm (inner diameter 12 mm, outer diameter 18 mm). The Lamé theory for thick-walled cylinders [16] is used to calculate the maximum internal pressure that the tube can withstand within the elastic range.

Consider a thick-walled cylinder with inner radius r_i and outer radius r_o under an internal pressure p_1. The hoop stress is highest at the inner wall, and the Lamé solution is

$$\sigma_{\theta,\text{inner}} = p_1 \frac{r_o^2 + r_i^2}{r_o^2 - r_i^2} \tag{1}$$

Here, $\sigma_{\theta,\text{inner}}$ is the hoop stress at the inner wall of the all-metal seal tube (MPa), and p_1 is its internal pressure (MPa). The outer radius is $r_o = 9$ mm (outer diameter 18 mm), and the inner radius is $r_i = 6$ mm (inner diameter 12 mm). Setting the inner-wall hoop stress equal to the yield strength $\sigma_{ys} = 170$ MPa gives the maximum elastic pressure-bearing capacity of the 3 mm thick tube:

$$p_{max} = \frac{\sigma_{ys}(r_o^2 - r_i^2)}{r_o^2 + r_i^2} = \frac{170 \times (9^2 - 6^2)}{9^2 + 6^2} = \frac{170 \times 45}{117} \approx 65.4 \text{ MPa} \tag{2}$$

The maximum elastic pressure-bearing capacity of the 3 mm thick all-metal seal tube is only 65.4 MPa. This is about 37.4% of the 175 MPa proof pressure, i.e., about 2.68 times lower. It is even lower than the 70 MPa working pressure. Simply increasing the wall thickness to close this gap would raise the mass and volume substantially. It would also widen the non-magnetic gap and increase the reluctance, degrading the lightweight performance and the dynamic response of the solenoid valve. Therefore, the all-metal scheme is not a preferable option for solenoid-valve seal tubes with weight and volume constraints.

3.2. Mechanical Calculation of the Composite Structure

The macroscopic mechanical performance of the composite layer depends on the fiber, the matrix, and the winding process. For a hoop-wound layer, the hoop tensile strength is the key parameter determining its load-bearing capacity. It is estimated using the rule of mixtures [18]:

$$\sigma_{c,ult} = \sigma_{f,ult} V_f \eta \tag{3}$$

Here, $\sigma_{c,ult}$ is the hoop ultimate tensile strength of the composite layer (MPa). $\sigma_{f,ult}$ is the tensile strength of the fiber tow (4100 MPa for the HTA40-grade carbon fiber). V_f is the fiber volume fraction (0.55 to 0.65 for wet winding, with 0.6 adopted in this work). η is the fiber strength conversion efficiency, which accounts for process damage, fiber buckling, and imperfect straightness (0.82 adopted). Substituting the values gives

$$\sigma_{c,ult} = 4100 \times 0.60 \times 0.82 \approx 2017.2 \text{ MPa} \tag{4}$$

The yield strength of S31603 stainless steel is 170 MPa, whereas the hoop ultimate tensile strength of the HTA40-grade carbon-fiber composite layer calculated by the rule of mixtures can reach 2017.2 MPa. Even considering the process reduction and the safety factor, its allowable hoop stress remains at a high level. The two differ by an order of magnitude in their capacity to carry the hoop load, which is the fundamental mechanical basis for the carbon-fiber winding layer to effectively share the internal pressure load and significantly reduce the stress in the metallic liner.

The macro-scale elastic constants of the composite layer are also estimated by the rule of mixtures. The hoop elastic modulus is given by

$$E_1 = \eta\left[E_f V_f + E_m\left(1 - V_f\right)\right] \tag{5}$$

Here, E_f is the tensile modulus of the carbon fiber (240 GPa), and E_m is the elastic modulus of the epoxy resin matrix (3 GPa [22]). V_f is the fiber volume fraction (0.6), and η is the fiber strength conversion efficiency (0.82). Substituting the values gives

$$E_1 = 0.82 \times (240 \times 0.60 + 3.0 \times 0.4) \approx 119 \text{ GPa} \tag{6}$$

The radial and axial elastic moduli are governed by the transverse modulus perpendicular to the fiber direction and are estimated by the inverse rule of mixtures.

$$E_2 = E_3 = \frac{1}{\frac{V_f}{E_{fT}} + \frac{1-V_f}{E_m}} \tag{7}$$

Here, E_{fT} is the transverse elastic modulus of the carbon fiber (15 GPa [23]). Substituting the values gives

$$E_2 = E_3 \approx 5.8 \text{ GPa} \tag{8}$$

Erturk and Acikgoz [24] compared analytical and numerical homogenization methods for carbon-fiber/epoxy laminae. They found the longitudinal modulus to be nearly method-independent, whereas the transverse modulus and, above all, the shear modulus depend strongly on the method. The present constants are therefore conservative: E_1 from the rule of mixtures, E_2 and E_3 from the inverse rule of mixtures, and G_{12}, G_{13}, and G_{23} from established lamina data [25–27].

3.3. Preliminary Thickness-Selection Model Based on Force Equilibrium

3.3.1. Load-Distribution Model

The metallic liner and the composite layer are regarded as a tightly bonded combined thick-walled cylinder. Under a uniform proof pressure, the total load is shared by the two.

The equivalent pressures shared by the composite layer and the metallic liner are denoted as below.

$$p = p_c + p_m \tag{9}$$

where the proof pressure is 175 MPa, and the symbols denote the equivalent pressures shared by the metallic liner and the composite layer, respectively.

3.3.2. Load-Bearing Limit of the Metallic Liner

In the composite structure, the metallic liner and the carbon-fiber layer carry the load together. The carbon-fiber layer bears most of the hoop load, so the liner only bears part of the internal pressure. The pressure acting on the metallic liner under extreme conditions is set so that the hoop stress at its inner wall just reaches the yield strength. The geometry is the same as in Section 2.1, so the Lamé solution of Equation (1) applies, with the internal pressure replaced by the pressure p_m that the liner bears on its own. Setting the inner-wall hoop stress equal to the yield strength then gives the maximum pressure that the metal layer can support independently:

$$p_{m,max} = \frac{\sigma_{ys}\left(r_m^2 - r_i^2\right)}{r_m^2 + r_i^2} = \frac{170 \times \left(8^2 - 6^2\right)}{8^2 + 6^2} = \frac{170 \times 28}{100} = 47.6 \text{ MPa} \tag{10}$$

where $r_m = 8$ mm (outer diameter 16 mm) and $r_i = 6$ mm (inner diameter 12 mm) are the outer and inner radii of the metallic liner, respectively. That is, when the pressure independently borne by the liner reaches $p_{m,max}$, the hoop stress at its inner wall just reaches the yield strength. Owing to the constraint of the carbon-fiber layer, the liner in the real composite structure is in a better stress state than under independent pressure. Local yielding is confined to an extremely thin surface layer and cannot develop into overall plastic collapse.

3.3.3. Determination of the Composite Layer Thickness

The part of the proof pressure that exceeds the load-bearing capacity of the metallic liner is borne by the composite layer, that is

$$p_c = p - p_{m,max} = 175 - 47.6 = 127.4 \text{ MPa} \tag{11}$$

For a hoop-wound layer, the entire hoop load can be assumed to be carried by the fiber (composite netting theory) [17,18]. At the outer radius of the liner, the hoop force equilibrium per unit length is

$$\sigma_{c,ult}\, t_c = p_c\, r_m \tag{12}$$

Here, $\sigma_{c,ult}$ is the hoop ultimate tensile strength of the composite layer (2017.2 MPa, calculated in Section 2.2). t_c is the total thickness of the composite layer (mm). p_c is the pressure that the composite layer must bear (127.4 MPa, from Equation (11)). r_m is the outer radius of the metallic liner (mm). From this, the required theoretical thickness is solved

$$t_c = \frac{p_c\, r_m}{[\sigma]_c} = \frac{127.4 \times 8}{2017.2} \approx 0.51 \text{ mm} \tag{13}$$

The calculation shows that a winding-layer thickness of about 0.51 mm is sufficient. At this thickness, the liner and the composite layer together satisfy the strength requirement at the 175 MPa proof pressure (working pressure 70 MPa, safety factor 2.5). Considering process fluctuation, long-term performance, and potential impact loads, a design margin is introduced in engineering practice, and the design thickness of the winding layer is adopted as 1 mm.

4. Finite Element Simulation Verification

A three-dimensional finite element model is established with ANSYS Workbench (ANSYS 2022 R2) to verify the theoretical design of the composite seal tube. Its stress distribution under the limit load is also examined [28].

4.1. Model Establishment

4.1.1. Geometric Model

According to the structural parameters determined in Section 3, a three-dimensional geometric model is established. The metallic liner has an inner diameter of 12 mm, an outer diameter of 16 mm, and a wall thickness of 2 mm. The composite reinforcement layer has an outer diameter of 18 mm and a total wall thickness of 1 mm (nine hoop-wound layers). It should be noted that the thickness of the composite reinforcement layer in the simulation model is taken as the nominal design value of 1 mm, corresponding to nine hoop-wound carbon-fiber layers. In the actual specimen, wet winding causes small fluctuations in resin impregnation and fiber lay-up. These produce a slightly uneven surface, so the measured average thickness is about 1.165 mm, a little larger than the nominal 1 mm. However, the number of load-bearing carbon-fiber layers remains nine, consistent with the design, and the fiber skeleton is unchanged. The number of fiber layers and the load-bearing mechanism used in the theoretical calculation and the finite element analysis therefore remain valid. The extra thickness comes from resin enrichment and does not reduce the load-bearing capacity of the seal tube. For comparison, an all-metal seal tube model with an inner diameter of 12 mm, an outer diameter of 18 mm, and a wall thickness of 3 mm is also established.

4.1.2. Element Type and Meshing

Hexahedral structured meshing is used, with local refinement at the inner wall of the metallic liner and at the interface between the composite layers; the local target element size is 0.02 mm. The resulting mesh contains approximately 2,100,000 elements and about 3,200,000 nodes, and its average orthogonal quality, skewness and aspect ratio are 0.86, 0.19 and 1.7, respectively.

4.1.3. Material Properties

The material of the all-metal seal tube is S31603 stainless steel, and the metallic liner of the composite seal tube is also made of S31603 stainless steel. Both the all-metal seal tube and the metallic liner adopt the same S31603 stainless steel material model. In the elastic stage, an isotropic linear-elastic relation is used, with an elastic modulus of 195 GPa and a Poisson's ratio of 0.30. In the plastic stage, a bilinear isotropic-hardening model based on the von Mises yield criterion is adopted, with an initial yield stress of 170 MPa. The composite reinforcement layer is defined as an orthotropic elastic material, and the specific parameters are listed in Table 2. To describe the material orientation of the hoop-wound fibers, which varies with the circumferential position, a local cylindrical coordinate system coaxial with the cylinder is established and assigned to the composite solid. The local X, Y, and Z directions correspond to the radial, hoop, and axial directions, respectively, with elastic moduli of 5.8, 119, and 5.8 GPa. The direction indices in the material parameter table are defined as 1—hoop, 2—radial, and 3—axial.

4.1.4. Contact Settings

A bonded contact is defined between the outer surface of the metallic liner and the inner surface of the composite layer, which represents an ideal bonding state and neglects interface debonding and slip. Since no slip or debonding was observed between the two layers in

the actual tests, the results at 175 MPa should be understood as corresponding to such ideal bonding conditions.

Table 2. Material parameters of the seal tube.

Stainless Steel Material	Composite Reinforcement Layer
Material: S31603 stainless steel (ASTM A479/A479M-25 [6])	Fiber: Toho Tenax HTA40 E15 1K carbon fiber [20]
Yield strength: 170 MPa	Hoop elastic modulus: 119 GPa
Elastic modulus: 195 GPa	Radial elastic modulus: 5.8 GPa
Poisson's ratio: 0.30	Axial elastic modulus: 5.8 GPa
	Poisson's ratio: 0.28 (hoop-radial) [25]
	Poisson's ratio: 0.28 (hoop-axial)
	Poisson's ratio: 0.40 (radial-axial)
	Shear modulus: 4.5 GPa (hoop-radial) [26]
	Shear modulus: 4.5 GPa (hoop-axial)
	Shear modulus: 3.5 GPa (radial-axial) [27]
	Hoop ultimate tensile strength: 2017.2 MPa

4.2. Loads and Boundary Conditions

A three-dimensional cylinder model without the end-cap solid is established, with the cylinder axis taken as the z direction. A uniform internal pressure $P_1 = 175$ MPa is applied to the inner surface of the metallic liner. A uniform external pressure $P_2 = 0.1$ MPa is applied to the outer surface of the composite layer to represent the external atmosphere. Both pressures are expressed as absolute pressures, corresponding to a pressure difference of 174.9 MPa, and they act normal to the respective surfaces. A fixed support is applied to the bottom annular end face of the metallic liner. It constrains the three translational degrees of freedom of the nodes on this face ($U_z = U_x = U_y = 0$). No separate displacement constraint is applied to the composite reinforcement layer; its displacement is coordinated through the contact relationship with the metallic liner. Apart from this fixed support, no other displacement constraint is applied to the model. A steady-state analysis is adopted, and the load is applied by ramp increments in 10 substeps up to the target value. Overall equilibrium is verified by comparing the axial reaction force at the fixed end with the resultant of the applied axial load.

4.3. Result Analysis

4.3.1. Simulation Results for the All-Metal Seal Tube

To reveal the load-bearing mechanism of the composite seal tube, a comparative analysis is first carried out on the all-metal seal tube (wall thickness 3 mm). At a proof pressure of 175 MPa, the calculation results for the all-metal seal tube are shown in Figure 2. The maximum equivalent stress is 468.26 MPa at the inner wall. This is far above the yield strength of S31603 (170 MPa), so the all-metal scheme undergoes extensive plastic yielding at this pressure. The maximum deformation is 0.67 mm, occurring at the outer wall at the middle of the seal tube, and is an unrecoverable plastic deformation.

This result confirms the theoretical prediction that the all-metal scheme cannot meet the strength requirement at the 175 MPa proof pressure. It also provides a baseline for the comparison with the composite seal tube.

4.3.2. Simulation Results for the Composite Seal Tube

(1) Stress of the metallic liner

At a proof pressure of 175 MPa, the stress distribution of the metallic liner in the composite seal tube exhibits the following characteristics. The maximum equivalent stress

at the inner wall is about 250 MPa. Although this value exceeds the yield strength of S31603 (170 MPa), it is a local surface effect because the inner wall directly bears the 175 MPa internal pressure. A relatively high local stress concentration therefore unavoidably occurs on the material surface. Along the wall-thickness direction, the equivalent stress decays rapidly, and the stress level in most of the liner region is below the yield strength. More importantly, owing to the strong constraint of the outer carbon-fiber layer, the overall deformation of the metallic liner is strictly limited. Even if the inner wall locally yields, the plastic zone is confined to an extremely thin surface layer and does not develop into overall plastic collapse.

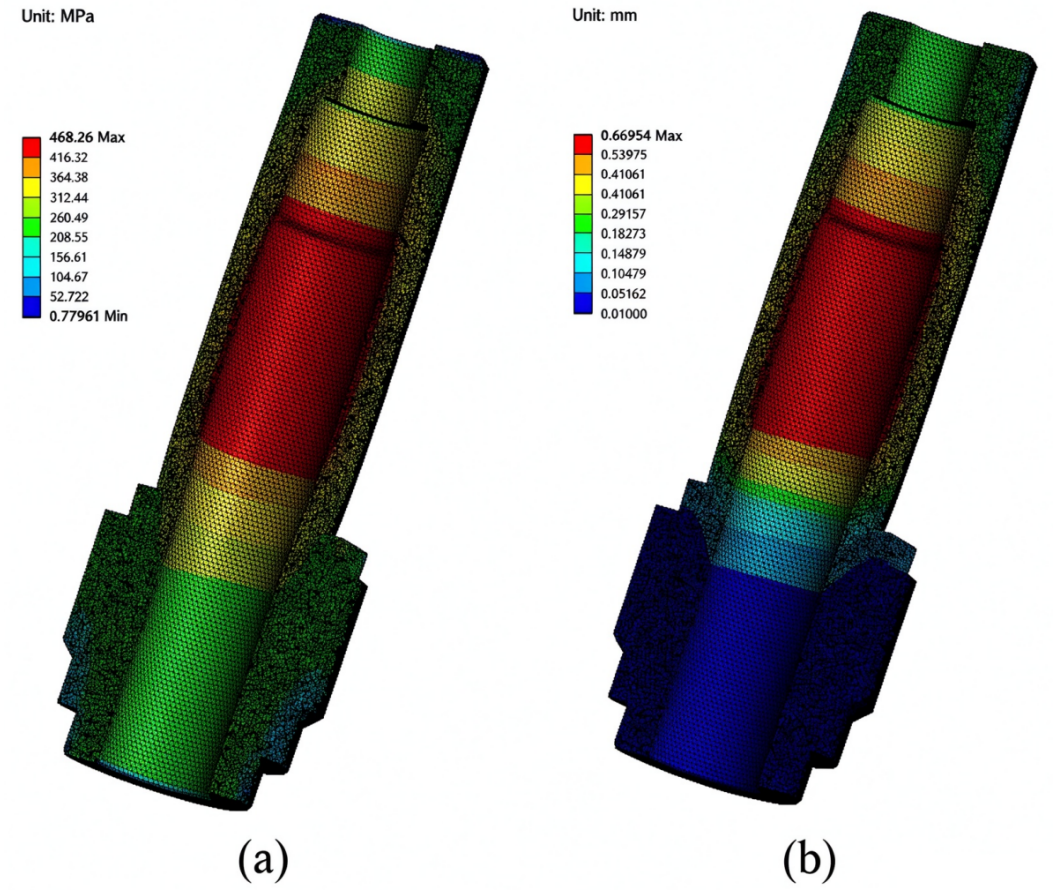


Figure 2. Simulation results of the all-metal seal tube: (**a**) equivalent stress contour; (**b**) total deformation contour.

The carbon-fiber layer carries most of the hoop load and, through interface bonding, applies a radial compressive stress to the metallic liner, which restrains its tendency to expand in the hoop direction. The high stress at the inner wall is an inevitable result of the direct internal pressure action, while the load-bearing role of the carbon-fiber layer ensures the overall safety of the structure.

(2) Stress of the composite reinforcement layer

The composite reinforcement layer is dominated by the hoop stress. The maximum hoop stress is about 728.5 MPa and occurs in the innermost carbon-fiber layer. This value is below its ultimate tensile strength (2017.2 MPa), giving a safety margin of about 63.9%. The composite layer therefore remains in an elastic and safe state at the proof pressure.

(3) Deformation analysis of the composite seal tube

At a proof pressure of 175 MPa, the maximum deformation is 0.115 mm at the inner wall and 0.08 mm at the outer wall. Both values are far smaller than the 0.67 mm of the all-metal seal tube. This result demonstrates the strong constraint effect of the carbon-fiber winding layer on the metallic liner. Under internal pressure, the liner tends to expand. The carbon-fiber layer holds it through its high hoop stiffness (119 GPa) and high strength (2017.2 MPa), so the overall deformation stays extremely small. The minor plastic strain caused by the local stress concentration at the inner wall is confined to an extremely thin surface layer, see Figure 3.

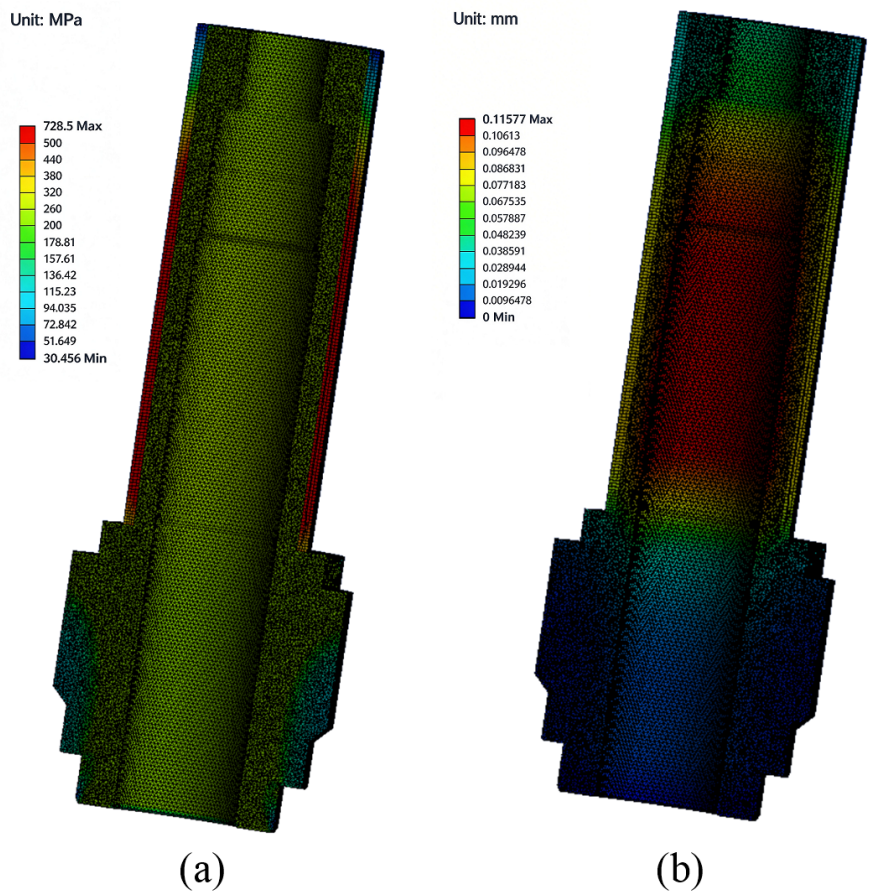


Figure 3. Simulation results of the composite seal tube: (**a**) equivalent stress contour; (**b**) total deformation contour.

4.3.3. Simulation Comparison Between the All-Metal and Composite Schemes

The simulation results of the all-metal seal tube and the composite seal tube are compared in Table 3.

Table 3. Comparison of the simulation results of the all-metal and composite schemes.

Comparison Item	All-Metal Seal Tube	Composite Seal Tube
Maximum equivalent stress	468.26 MPa (far above yield)	250 MPa at the inner wall (local)
Maximum deformation	0.67 mm	0.115 mm (inner wall)/0.08 mm (outer wall)
Structural state	Extensive plastic yielding	Overall load-bearing safety (minor local plasticity)
Safety margin	Does not meet requirement	Meets the design requirement

4.4. Simulation Summary of the All-Metal and Composite Schemes

The deformation between the metallic liner and the composite reinforcement layer is continuous, and the displacement difference at the interface is extremely small. During load bearing, the two layers achieve good deformation coordination and synergistic work. The inner wall of the composite seal tube directly bears the 175 MPa internal pressure, so a local stress concentration occurs there. Even so, the overall maximum deformation is extremely small. This trend stems from the strong constraint of the carbon-fiber winding layer on the metallic liner. When the liner tends to expand under internal pressure, the carbon-fiber layer holds the liner through its high stiffness and high strength, strictly confining the deformation to an extremely small range.

Based on the above analysis, the composite seal tube has a sufficient safety margin at a proof pressure of 175 MPa. The metallic liner has a local high-stress zone at the inner wall. However, the carbon-fiber layer constrains it strongly, the overall deformation remains extremely small, and structural integrity is maintained. The maximum stress of the composite layer is about 36.1% of its ultimate strength, providing a safety margin of about 63.9%. Limit-load analysis and burst tests can be further carried out to determine the actual burst pressure of the structure. According to the existing simulation and proof-test results, the burst pressure is expected to be much higher than the proof pressure of 175 MPa.

5. Pressure Test of the Seal Tube

To verify the actual load-bearing performance of the composite seal tube, comparative pressure tests are carried out on the self-designed composite seal tube and the conventional all-metal seal tube. The tests use a self-developed oil-bladder-driven ultra-high-pressure test device. Through medium isolation and quick-connect interface design, the device achieves high-pressure assessment of the specimen while ensuring safety. The pressure-test equipment, the explosion-proof tank, and the pressure-test conditions of the two groups of specimens are shown in Figure 4.

5.1. Test Specimens and Conditions

Two groups of comparison specimens are set up. The reference group is the all-metal seal tube designed conventionally and made of S31603 stainless steel. The experimental group is the composite seal tube proposed in this paper, consisting of an S31603 stainless steel liner with a wall thickness of 2 mm (outer diameter 16 mm) and an external HTA40 carbon-fiber composite reinforcement layer. The key geometric and mass parameters of the two groups are listed in Table 4.

The designed geometric parameters of the two groups are kept consistent, with the main differences lying in the material system and the mass distribution. Although slight deviations exist in some dimensions due to differences in the manufacturing process, both groups satisfy the test requirements at the proof pressure of 175 MPa in their respective independent test systems.

The composite seal tube specimen is wound with nine layers of carbon fiber. During actual forming, because of the capillary effect of resin infiltration and the uneven residual resin, slight undulations occur on the surface of the wound layer, so the final outer diameter is slightly larger than the theoretical value.

The tests use a stepwise pressure-increase method. The pressure is first slowly increased from 0 MPa to 100 MPa for preloading. After confirming no leakage, the pressure is then increased stepwise to the proof pressure of 175 MPa, with the specimen deformation monitored throughout. The comparison of the two groups of specimens is shown in Figure 5.

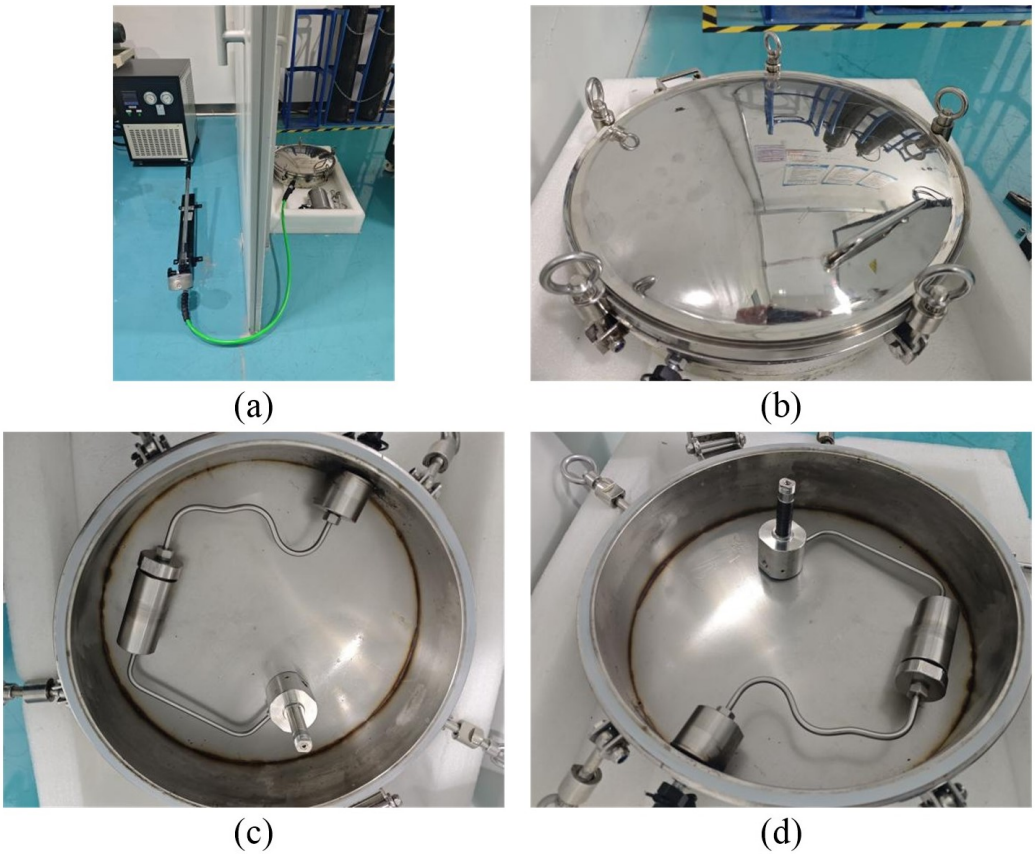


Figure 4. Pressure-test setup and test scenes: (**a**) pressure-test equipment; (**b**) explosion-proof tank; (**c**) pressure test of the metal seal tube; (**d**) pressure test of the composite seal tube.

Table 4. Comparison of the key parameters of the test specimens.

Parameter	Metal Seal Tube (Reference)	Composite Seal Tube (Experimental)
Material	S31603 stainless steel	S31603 liner + HTA40 carbon-fiber winding layer
Inner diameter (mm)	12.00	12.00
Outer diameter before test (mm)	18.03	18.33
Total wall thickness (mm)	3.00 (all metal)	2.00 (liner) + 1.165 (composite layer)
Height (mm)	65.52	66.81
Mass (g)	177.69	161.19

Note: The composite reinforcement layer thickness of 1.165 mm in Table 4 is the measured value after actual forming of the specimen. The resin distribution in wet winding is not uniform, so the winding-layer surface is slightly undulating. The measured thickness is therefore a little larger than the nominal 1 mm. However, the number of load-bearing carbon-fiber winding layers is still nine, as determined by the design, consistent with the finite element model. The surface undulations only cause resin enrichment and do not affect the load-bearing capacity of the fiber skeleton.

5.2. Design and Analysis of the Winding Tension

5.2.1. Breaking Strength of the Fiber Tow

The winding tension is a key process parameter affecting the quality of the composite layer, fiber damage, and residual stress [17]. Its reasonable value should be based on the breaking strength of the fiber tow. The 1K carbon-fiber tow used in this paper consists

of 1000 filaments, each with a diameter of 7 μm, so the cross-sectional area of the fiber tow is

$$A = 1000 \times \pi \times \left(3.5 \times 10^{-3}\right)^2 \approx 0.0385 \text{ mm}^2 \quad (14)$$

The breaking strength of the fiber tow is calculated using the rule-of-mixtures strength [18]:

$$F_{break} = \sigma_{f,ult} A = 4100 \times 0.0385 \approx 157.9 \text{ N} \quad (15)$$



Figure 5. Comparison of the metal seal tube and the composite seal tube.

5.2.2. Safe Tension Window

To prevent excessive wear and fracture of the fiber during winding, the process tension is usually controlled at 1–5% of the breaking strength [17]. For a fine 1K tow, the lower end of the interval should be preferred to ensure winding safety. The safe tension window thus determined is

$$F_{tension} = (1\% \text{ to } 5\%)\, F_{break} = 1.579 \text{ to } 7.895 \text{ N} \quad (16)$$

Given the sensitivity of the 1K fine tow to fiber damage, the actual winding tension is set to 7 N, which is about 4.4% of the breaking strength, near the lower end of the safe window. This ensures process safety while maintaining a stable fiber volume fraction.

5.2.3. Layer-by-Layer Tension Reduction Strategy

To prevent the inner-layer fibers from being crushed or loosened by the shrinkage of the subsequently wound layers, which would cause an uneven interlayer stress distribution after curing, the winding tension adopts a tight-inside-and-loose-outside layer-by-layer reduction scheme. The tension of the first layer is 7 N and decreases by 0.3 N per layer thereafter, until the outermost layer reaches about 4.3 N. This scheme keeps the inner-layer fibers in a relatively high tension state while the outer-layer tension gradually decreases, which is conducive to the synergistic load sharing of all the layers after curing.

5.2.4. Estimation of the Number of Winding Layers

The single-layer thickness of wet hoop winding depends on the fiber specification, winding tension, and resin content. The cross-sectional area of the 1K carbon-fiber tow used in this paper is about 0.0385 mm^2, the measured tow thickness is about 0.07 mm, and the calculated band width is about 0.55 mm. The single-layer thickness commonly used in wet winding is 0.10 to 0.15 mm [17]. Taking an average single-layer thickness of 0.12 mm, the required number of winding layers is

$$N = \frac{t_{c,design}}{0.12} \approx 8.3 \text{ layers} \quad (17)$$

The nominal thickness of the reinforcement layer is taken as 1 mm, corresponding to nine winding layers. After the actual specimen was wound with nine layers, the non-uniform distribution of resin on the fiber-bundle surface during wet winding produced slight protrusions on the outer surface of the winding layer. The measured total thickness is about 1.165 mm, corresponding to an outer diameter of 18.33 mm, which agrees with the measured values in Tables 4 and 5. This deviation is caused by process-induced surface unevenness. The number of load-bearing layers is still the designed nine, so the nominal load-bearing capacity is unchanged.

Table 5. Comparison of radial deformation under a pressure of 175 MPa.

Indicator	**Metal Seal Tube (Reference)**	**Composite Seal Tube (Experimental)**
Outer diameter before test (mm)	18.03	18.33
Outer diameter after unloading (mm)	18.83	18.34
Outer diameter change (mm)	0.80	0.01
Deformation rate (%)	4.4	≈0.05
Deformation nature	Permanent plastic deformation	Minor residual deformation

5.3. Test Results and Comparative Analysis

5.3.1. Radial Deformation and Load-Bearing Capacity

The radial deformation results of the two groups of specimens under a pressure of 175 MPa are shown in Table 5.

At the proof pressure of 175 MPa, the all-metal seal tube deformed irreversibly and failed in a single test: its outer diameter expanded permanently from 18.03 mm to 18.83 mm, an unrecoverable plastic deformation of about 0.80 mm (4.4%), indicating that the material had yielded and that the load-bearing capacity had reached its limit. The failure mode is consistent with the prediction of the elastic–plastic finite element analysis. The composite seal tube was then subjected to three cycles of pressurization, holding, unloading and measurement at the proof pressure of 175 MPa, and the outer diameter change after the final unloading was taken as the test result. After unloading, the outer diameter of the composite seal tube increases only from 18.33 mm to 18.34 mm, with a residual deformation of about 0.01 mm (about 0.05%). No cumulative plastic deformation occurred over the three cycles, which shows that the carbon-fiber reinforcement layer effectively shares the hoop stress. Even if the metallic liner undergoes minor plastic deformation, it is strictly

confined to an extremely thin surface layer, and the structure exhibits good dimensional stability and load-bearing capacity, as shown in Figure 6.

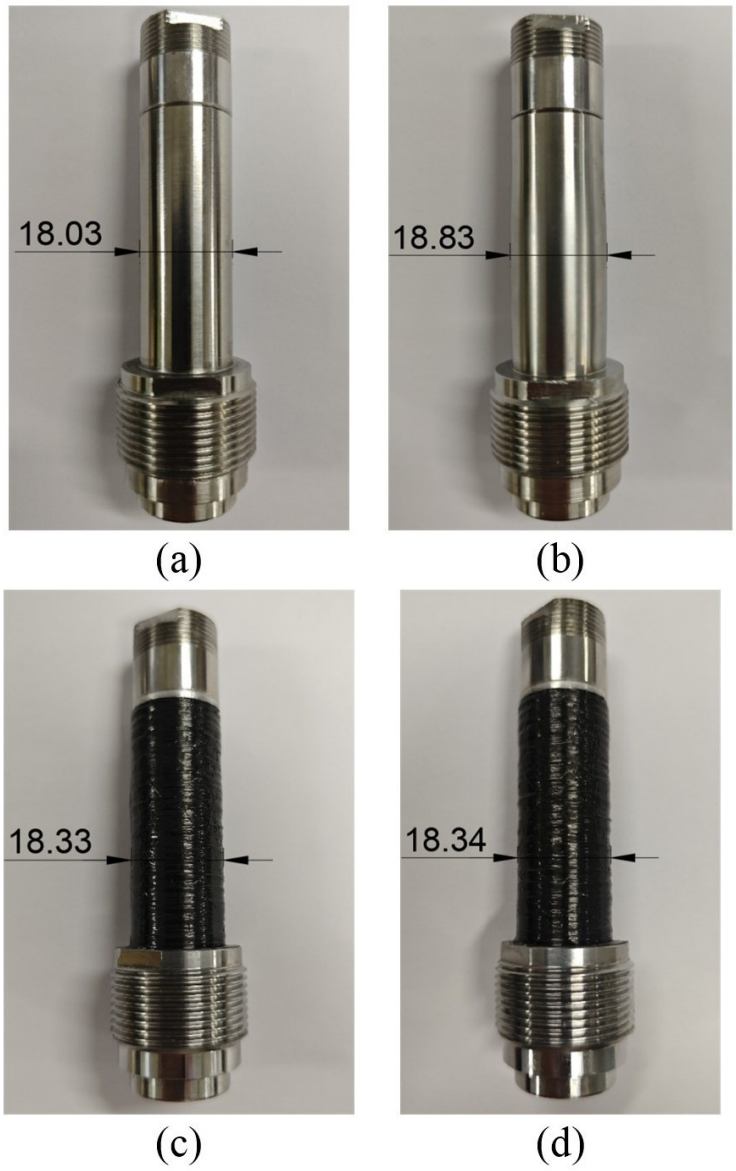


Figure 6. Outer diameters before and after the test: (**a**) metal tube before; (**b**) metal tube after; (**c**) composite tube before; (**d**) composite tube after. The arrows indicate the dimension annotations for the measured outer diameter (values in mm).

5.3.2. Axial Deformation

The axial dimension changes of the two groups of specimens before and after the test are shown in Table 6.

Table 6. Comparison of the axial deformation before and after the test.

Indicator	Metal Seal Tube (Reference)	Composite Seal Tube (Experimental)
Height before test (mm)	65.52	66.81
Height after test (mm)	65.54	66.81
Axial change (mm)	<0.03	0
Nature of change	Negligible	Undeformed

The length changes of both seal tubes are less than 0.03 mm and are negligible. Under the given end-constraint conditions, the pressure does not cause significant axial permanent deformation.

5.3.3. Lightweight Benefit

The load-bearing capacity is greatly improved: overall plastic yielding is replaced by minor plastic deformation of the inner surface. At the same time, the mass of the composite seal tube is about 9.3% lower than that of the metal seal tube, achieving the goal of stronger and lighter. The lightweight benefit is shown in Table 7.

Table 7. Comparison of the lightweight benefit.

Indicator	Metal Seal Tube (Reference)	Composite Seal Tube (Experimental)	Change
Mass (g)	177.69	161.19	−16.50
Weight-reduction ratio	Baseline	N/A	About 9.3%

N/A, not applicable.

5.4. Solenoid-Valve Performance Test

To evaluate the applicability of the composite seal tube in an actual solenoid valve, gas-tightness and valve-opening performance tests are carried out using the MPAPOWER ultra-high-pressure solenoid-valve test system (Shanghai MPA Fluid Power Co., Ltd., Shanghai, China). The test system consists of a pressure-boosting control box and an explosion-proof test box. Nitrogen is used as the pressurizing medium. A two-stage gas booster pump (stage 1, AMG152, up to 90 MPa; stage 2, AG-303, up to 150 MPa) provides a maximum output of 150 MPa. The processes are coordinated by a Siemens S7-1200 PLC and an industrial PC. The system can perform high-pressure tests, valve-opening tests, and leakage tests. The ultra-high-pressure solenoid-valve test system and the installation of the high-pressure switching solenoid valve are shown in Figure 7.



(a) (b)

Figure 7. Solenoid-valve test system: (**a**) MPAPOWER ultra-high-pressure test system; (**b**) solenoid valve installed in the explosion-proof test box.

5.4.1. Gas-Tightness Performance Test

To verify the sealing reliability of the composite seal tube, long-duration pressure-holding leakage tests are carried out at several pressure levels. The results are shown in Table 8.

The gas-tightness tests are conducted at two pressure levels. The first level is 12.3 MPa with a pressure-holding time of 20 min, and the second level is 105 MPa with a pressure-holding time of 38 min. During the test, the solenoid valve is first kept closed to monitor

its gas-tightness capability. After the pressure stabilizes and shows no obvious change, the solenoid valve is energized and opened, allowing the gas to flow into the downstream pipeline. The system then performs pressure replenishment. Thus, in the pressure–time curve of the gas-tightness test, a brief pressure-drop-and-recovery inflection point appears. This is a normal response to the gas flow and the system pressure replenishment at the instant of valve opening. Apart from the transient pressure fluctuation caused by the valve-opening action, the pressure gauge reading shows no observable fluctuation during the rest of the pressure-holding time. The gas-tightness performance therefore satisfies the design requirements, as shown in Figures 8 and 9.

Table 8. Gas-tightness performance test results at different pressure levels.

Test Pressure (MPa)	Pressure-Holding Time (min)	Change in Gauge Reading	Assessment
12.3	20	No obvious change	Meets the requirement
105	38	No obvious change	Meets the requirement

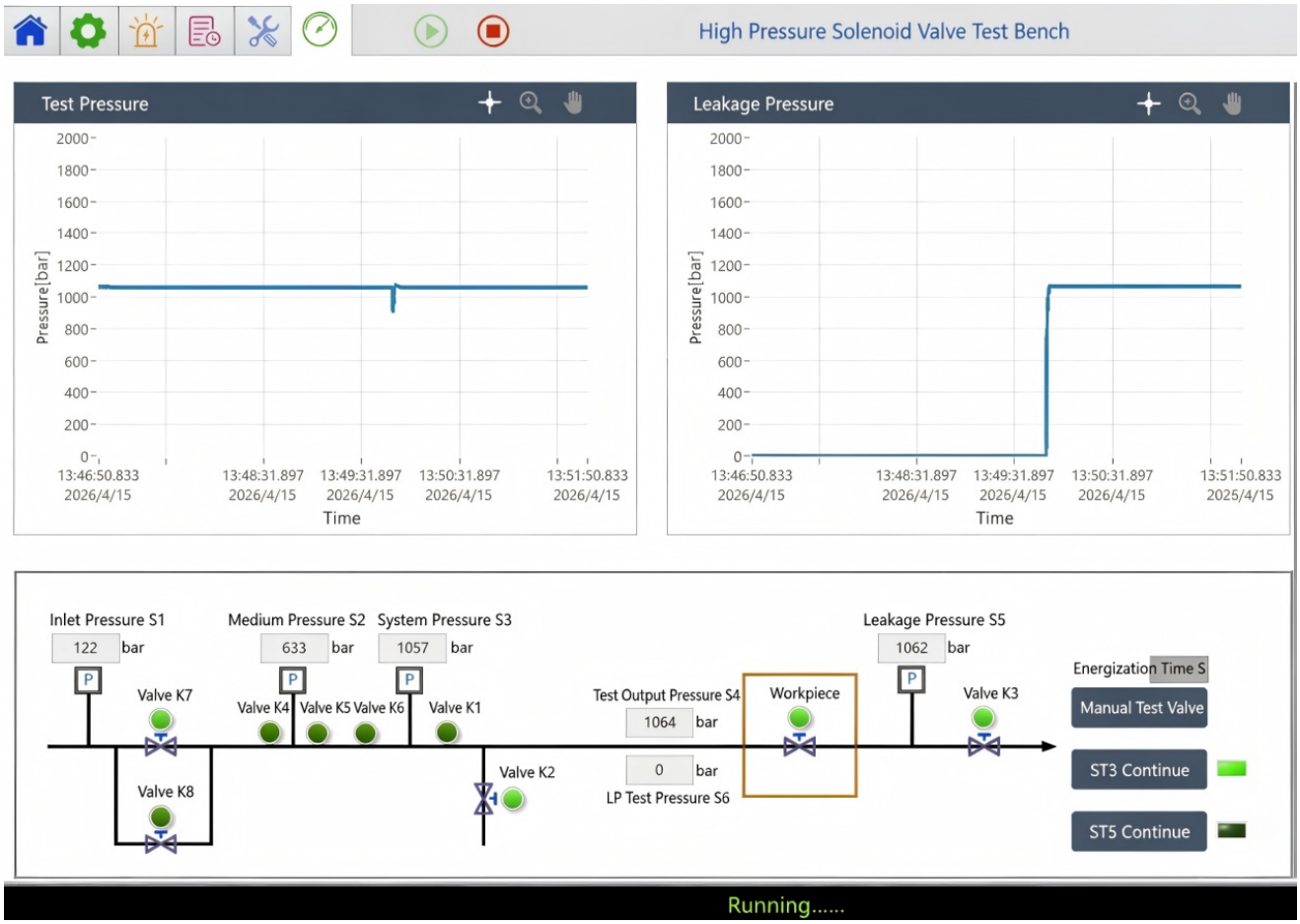


Figure 8. Gas-tightness test operation interface of the solenoid-valve test system.

5.4.2. Solenoid-Valve-Opening Performance Test

To verify the compatibility of the composite seal tube structure with the magnetic-circuit system of the solenoid valve, valve-opening performance tests are carried out at 0, 70, 80, 90, and 100 MPa. The solenoid valve opens normally at every test pressure, and all the results meet the design requirements. This confirms that the composite seal tube structure is compatible with the magnetic-circuit system of the solenoid valve, see Figure 10.

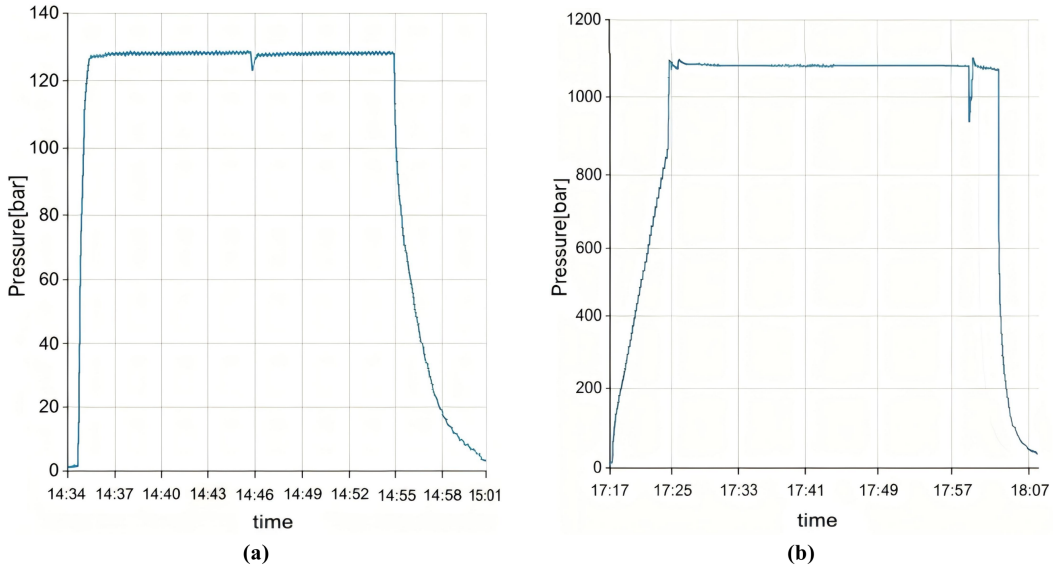


Figure 9. Gas-tightness test results (pressure–time curves): (**a**) low-pressure test; (**b**) high-pressure test.

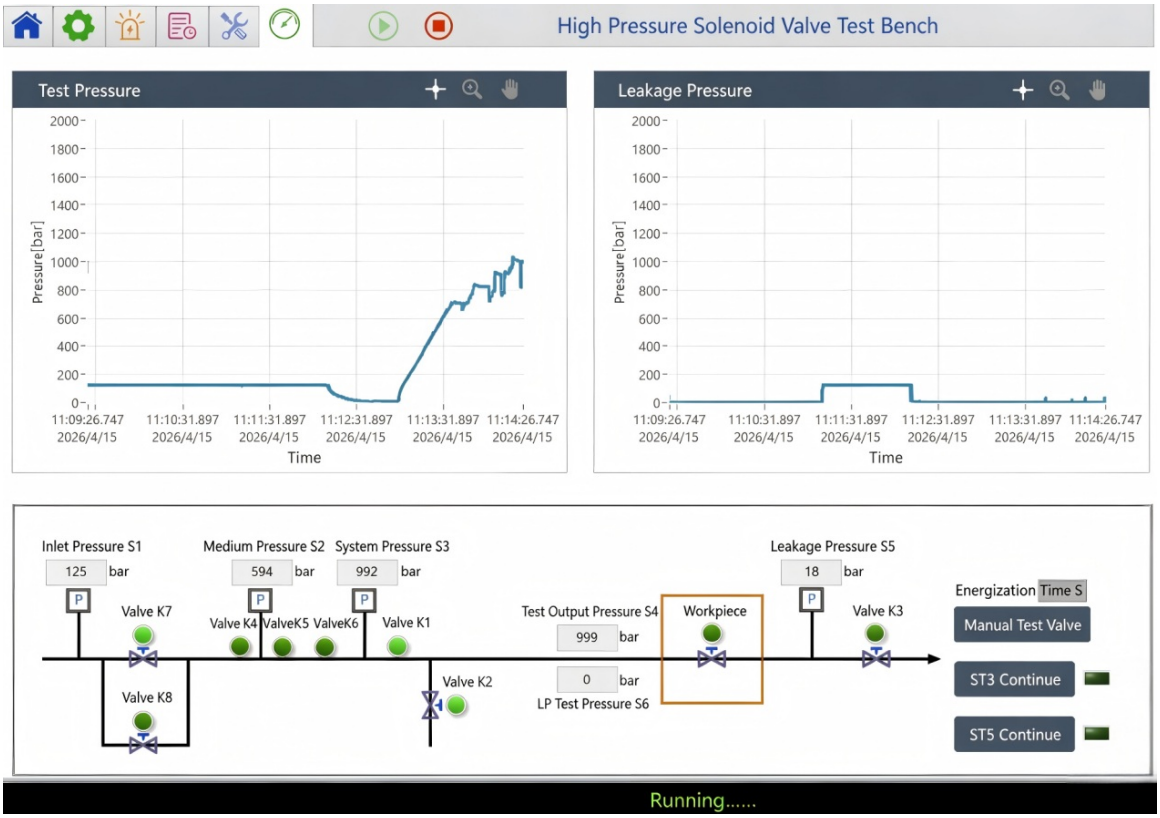


Figure 10. High-pressure valve-opening test: operation interface together with the opening performance result (pressure–time curve).

5.5. Comprehensive Analysis of the Test Results

The above test results can be summarized from five perspectives. First, in terms of load-bearing capacity, the composite seal tube shows a residual deformation of only about 0.01 mm after unloading from the 175 MPa proof pressure. The metal seal tube shows 0.80 mm of permanent plastic deformation at the same pressure. Second, in terms of dimensional stability, the composite seal tube essentially returns to its original shape after unloading, whereas the metal seal tube undergoes an irreversible expansion of 4.4%. Third,

in terms of lightweighting, the mass of the composite seal tube is reduced by about 9.3%. Fourth, in terms of sealing reliability, no leakage occurs over the long-duration pressure-holding tests at 12.3 MPa and 105 MPa. Fifth, in terms of magnetic-circuit compatibility, the solenoid valve still opens normally at 100 MPa. This indicates that the composite seal tube does not impair normal valve operation; a quantitative characterization of the electromagnetic performance was not part of this study. These results verify the feasibility and superiority of applying the carbon-fiber winding reinforcement scheme to the metal seal tube of an ultra-high-pressure hydrogen solenoid valve.

6. Comprehensive Advantage Analysis of the Solenoid Valve Based on the Carbon-Fiber Winding Process

Compared with the conventional all-metal seal tube scheme, the carbon-fiber-wound reinforced composite seal tube offers distinct advantages in terms of lightweighting, magnetic-circuit performance, fatigue and environmental resistance, designability, and cost-effectiveness.

Carbon-fiber composite offers a lightweight advantage and an extremely high specific strength. By using the fiber to carry the dominant hoop load, the seal tube can satisfy the strength requirement without a substantial increase in the metal wall thickness, thereby significantly reducing the structural mass while ensuring the pressure-bearing capacity and leaving room for further lightweight and integrated design [19].

Carbon-fiber composites offer potential advantages in terms of magnetic-circuit compatibility. The relative permeability of the carbon-fiber/epoxy composite is close to unity, i.e., comparable to that of air, so that the winding layer merely adds about 1 mm of non-magnetic gap outside the metal tube; from the viewpoint of the electromagnetic properties of the material, its disturbance of the magnetic circuit is therefore very limited. The thin-walled metallic liner has a low reluctance, which helps to maintain a low-reluctance magnetic circuit. The functional verification that the solenoid valve opens normally at 100 MPa further confirms the compatibility of the structure with the valve under high pressure.

At the material level, carbon-fiber composites generally show good fatigue and environmental resistance [18,19]. They are therefore promising for the high-frequency on/off duty of solenoid valves. The composite layer also carries most of the hoop load and thus lowers the stress in the metallic liner. This may reduce the susceptibility to hydrogen embrittlement and extend the service life of the seal tube in a high-pressure hydrogen environment.

The winding layer has high designability and functional-integration potential. The winding angle, the number of layers, and the stacking sequence can all be adjusted. This gives flexible control over the stiffness and strength distribution and allows an equal-strength optimal design [17,28]. In addition, sensors such as optical fibers can be integrated into the winding layer to realize online monitoring of the structural state, providing conditions for intelligent operation and maintenance of the equipment.

The cost-effectiveness of the carbon-fiber material is favorable. Although the unit price of the carbon-fiber material is relatively high, the amount used is small, and the resulting lightweight, high-efficiency, and long-life benefits provide significant added value in high-end equipment. The wet filament-winding process is mature and highly automated, which is conducive to cost control in mass production [17].

7. Conclusions

The metal seal tube of a 70 MPa class ultra-high-pressure hydrogen solenoid valve faces a contradiction between structural strength and magnetic-circuit efficiency. To resolve this contradiction, this paper proposes a lightweight scheme in which a thin-walled metal seal tube is reinforced by hoop-wound carbon fiber. The scheme is studied systematically. The main conclusions are as follows.

(1) The finite element analysis shows that at the proof pressure only minor local plastic deformation occurs at the inner surface of the composite seal tube. It is constrained by the outer carbon-fiber layer. The stress of the composite layer satisfies the strength requirement. The results therefore indicate an adequate margin against the strength requirement.

(2) The pressure-test results show that, after unloading at the proof pressure of 175 MPa, the composite seal tube has a residual deformation of only about 0.01 mm. Under the same pressure, an all-metal seal tube with the same external dimensions and a 3 mm wall thickness undergoes about 0.80 mm (4.4%) of unrecoverable plastic deformation. The mass of the composite seal tube is reduced by about 9.3%. The solenoid valve can still open normally at a pressure of 100 MPa. These results verify the overall performance in load-bearing capacity, dimensional stability and lightweighting, and provide preliminary confirmation of the compatibility of the carbon-fiber winding layer with the functional requirements of the solenoid valve.

(3) The carbon-fiber winding reinforcement structure decouples the structural load-bearing function from the electromagnetic function. It therefore offers an effective route for the lightweight design of pressure-bearing components of hydrogen solenoid valves at higher pressure levels.

Author Contributions: Conceptualization, S.M. and G.G.; methodology, S.M., C.S. and T.W.; software, T.F.; validation, T.H. and K.S.; formal analysis, S.M. and T.F.; investigation, S.M., G.G., C.S. and T.W.; resources, S.M. and G.G.; data curation, T.F. and K.S.; writing—original draft preparation, S.M.; writing—review and editing, S.M., G.G., C.S., T.W., T.F., T.H. and K.S.; visualization, T.F. and T.H.; supervision, S.M. and G.G.; project administration, S.M.; funding acquisition, S.M. All authors have read and agreed to the published version of the manuscript.

Funding: This work was supported by the Ningbo Key Technology Research and Development Program (Grant No. 2024T006).

Data Availability Statement: The original contributions presented in this study are included in the article. Further inquiries can be directed to the corresponding author.

Conflicts of Interest: Authors Shanhai Mao and Guoyun Gu were employed by the company Yuyao Sanlixin Solenoid Valve Co., Ltd.; authors Changbo Shi and Tiexiang Wang were employed by Huanjiang Laboratory. The remaining authors declare that the research was conducted in the absence of any commercial or financial relationships that could be construed as potential conflicts of interest.

References

1. Zheng, J.Y.; Liu, X.X.; Xu, P.; Liu, P.; Zhao, Y.; Yang, J. Development of High Pressure Gaseous Hydrogen Storage Technologies. *Int. J. Hydrogen Energy* **2012**, *37*, 1048–1057. [CrossRef]
2. Zheng, J.Y.; Ma, K.; Zhou, W.M.; Hu, J.; Gu, C.H.; Hua, Z.L. High-Pressure Hydrogen Storage Vessels for Hydrogen Refueling Stations. *Press. Vessel Technol.* **2018**, *35*, 35–42. (In Chinese)
3. Luo, W. *Research on New Energy Hydrogen Storage Equipment*; China University of Petroleum (East China): Qingdao, China, 2021. (In Chinese)
4. Lee, H.R.; Ahn, J.H.; Kim, H.Y. Design of a Solenoid Actuator for a Cylinder Valve in a Fuel Cell Vehicle. *Appl. Sci.* **2016**, *6*, 288. [CrossRef]
5. Lee, H.R.; Ahn, J.H.; Shin, J.O.; Kim, H.Y. Design of Solenoid Actuator for FCV Cylinder Valve Considering Structural Safety. *J. Korean Soc. Manuf. Technol. Eng.* **2016**, *25*, 157–163. [CrossRef]
6. *ASTM A479/A479M-25* ; Standard Specification for Stainless Steel Bars and Shapes for Use in Boilers and Other Pressure Vessels. ASTM International: West Conshohocken, PA, USA, 2025.
7. Zheng, Y. *Study on the Hydrogen Embrittlement Resistance of 316L Stainless Steel Strengthened by Laser Peening*; Jiangsu University: Zhenjiang, China, 2017. (In Chinese)
8. Ayakdas, O. *Design and Development of the Composite Hydrogen Storage Tanks by Using Stochastic Optimization Methods*; Izmir Katip Celebi University: Izmir, Turkey, 2018.
9. Wang, J.Z.; Xue, L.P.; Ran, Z.H.; Fang, H.R.; Chen, E.F. Simulation Analysis of the Electromagnetic Force of a Solenoid Valve Based on ANSYS Multiphysics. *Missiles Space Veh.* **2014**, *6*, 65–68. (In Chinese)

10. Wang, H.; Xu, H.Y.; Wang, D.Y.; Peng, C.; Liu, X.X.; Yin, Y.B. Static Electromagnetic Force Analysis of a Pneumatic Switching Solenoid Valve for Hydrogen Vehicles. *Fluid Meas. Control* **2025**, *6*, 1–5. (In Chinese)
11. Alleima. One Grade, Two Conditions: Alleima HighN50 for Pumps and Valves. Available online: https://www.alleima.com/en/news-media/archive/2026/01/one-grade-two-conditions-alleima-highn50-for-pumps-and-valves/ (accessed on 12 August 2026).
12. Kim, H.J.; Heng, L.; Mun, S.D. Surface Polishing of an Inconel 625 Bar by a Super-Fast MAF Process for a Solenoid Valve Stem Used in a Hydrogen Tank. *Metals* **2024**, *14*, 242. [CrossRef]
13. Zheng, C.X.; Li, R.; Wang, L.; Wei, Z.X. Mechanical Analysis and Optimization Control of a Carbon-Fiber-Wound Aluminum-Liner Hydrogen Storage Vessel. *Chem. Eng. Mach.* **2013**, *40*, 51–55. (In Chinese)
14. Zhan, H.L.; Zhu, B.B.; Yue, Z.Z.; Chen, Q.L. Stress Analysis of a 70 MPa Aluminum-Liner Carbon-Fiber Fully Wound Hydrogen Cylinder for Vehicles. *Mod. Manuf. Eng.* **2018**, *12*, 114–118. (In Chinese)
15. Okano, H.; Takagi, S.; Ishikawa, N.; Matsubara, K.; Takano, T.; Kageyama, T.; Matsunaga, H. Safety Evaluation and Life Prediction of Hoop-Wrapped Steel-Liner Pressure Vessels with Carbon-Fiber-Reinforced Plastic in an Ultra-High-Pressure Hydrogen Environment. *Int. J. Press. Vessels Pip.* **2026**, *222*, 105874. [CrossRef]
16. Zheng, J.Y.; Sang, Z.F. *Process Equipment Design*, 4th ed.; Chemical Industry Press: Beijing, China, 2015. (In Chinese)
17. Peters, S.T.; Humphrey, W.D.; Foral, R.F. *Filament Winding: Composite Structure Fabrication*; SAMPE Publishing: Covina, CA, USA, 1991.
18. Jones, R.M. *Mechanics of Composite Materials*, 2nd ed.; Taylor & Francis: Philadelphia, PA, USA, 1999.
19. Du, S.Y. *Mechanics, Design, Application and Evaluation of Composite Materials and Structures*; Harbin Institute of Technology Press: Harbin, China, 2009. (In Chinese)
20. Teijin Carbon. Tenax Filament Yarn—Product Data Sheet: Tenax-J HTA40 E15 1K 67tex. Available online: https://www.teijincarbon.com/products/filament-yarn/ (accessed on 26 August 2026).
21. *GB/T 42536-2023*; Assembly Valve on High Pressure Hydrogen Storage Cylinder for Vehicles. China Standards Press: Beijing, China, 2023. (In Chinese)
22. Lu, J.J.; Zheng, C.X.; Wang, L.; Dai, Y.; Wang, Z.; Song, Z. T700 Carbon Fiber/Epoxy Resin Composite Material Hygrothermal Aging Model. *Materials* **2025**, *18*, 369. [CrossRef] [PubMed]
23. Hao, P.; Tang, N.; Tiscar, J.M.; Gilabert, F.A. Untapped Potential of Recycled Thermoplastic Blends in UD Composites via Finite Element Analysis. *Polymers* **2025**, *17*, 1168. [CrossRef] [PubMed]
24. Erturk, A.T.; Acikgoz, C. Performance Comparison of Analytical and Numerical Methods of Elastic Properties of Composite Micromechanics. In *Advances in Machinery, Materials Science and Engineering Application*; Chen, M., Zhang, Z., Ding, X., Ma, H., Eds.; Advances in Transdisciplinary Engineering; IOS Press: Amsterdam, The Netherlands, 2022; Volume 24, pp. 10–15. [CrossRef]
25. Soden, P.D.; Hinton, M.J.; Kaddour, A.S. Lamina Properties, Lay-Up Configurations and Loading Conditions for a Range of Fibre-Reinforced Composite Laminates. *Compos. Sci. Technol.* **1998**, *58*, 1011–1022. [CrossRef]
26. David-West, O.; Advani, A.G. An Experimental Study of the Behaviour of Sandwich Composite Panels under Low-Speed Loading. *J. Compos. Mater.* **2026**, *60, 2419–2435* . [CrossRef]
27. Kang, M.-H.; Choi, J.H.; Kweon, J.H. Fatigue Life Evaluation and Crack Detection of the Adhesive Joint with Carbon Nanotubes. *Compos. Struct.* **2014**, *108*, 417–422. [CrossRef]
28. Vasiliev, V.V.; Morozov, E.V. *Advanced Mechanics of Composite Materials and Structures*, 4th ed.; Elsevier: Amsterdam, The Netherlands, 2018.

Disclaimer/Publisher's Note: The statements, opinions and data contained in all publications are solely those of the individual author(s) and contributor(s) and not of MDPI and/or the editor(s). MDPI and/or the editor(s) disclaim responsibility for any injury to people or property resulting from any ideas, methods, instructions or products referred to in the content.